Alternative model of single-bubble sonoluminescence

Kyuichi Yasui
Department of Physics, Waseda University, 3-4-1 Ohkubo, Shinjuku, Tokyo, Japan
(Received 19 May 1997)

A model of single-bubble sonoluminescence (SBSL) is constructed. In the model, the temperature is assumed to be spatially uniform inside the bubble except at the thermal boundary layer near the bubble wall even at the strong collapse based on the theoretical results of Kwak and Na [Phys. Rev. Lett. **77**, 4454 (1996)]. In the model, the effect of the kinetic energy of gases inside the bubble is taken into account, which heats up the whole bubble when gases stop their motions at the end of the strong collapse. In the model, a bubble in water containing air is assumed to consist mainly of argon based on the hypothesis of Lohse *et al.* [Phys. Rev. Lett. **78**, 1359 (1997)]. Numerical calculations under a SBSL condition reveal that the kinetic energy of gases heats up the whole bubble considerably. It is also clarified that vapor molecules (H_2O) undergo chemical reactions in the heated interior of the bubble at the collapse and that chemical reactions decrease the temperature inside the bubble considerably. It is suggested that SBSL originates in thermal radiation from the whole bubble rather than a local point (the bubble center) heated by a converging spherical shock wave widely suggested in the previous theories of SBSL. [S1063-651X(97)04612-6]

PACS number(s): 78.60.Mq, 47.55.Bx

I. INTRODUCTION

Observations of a single-bubble sonoluminescence (SBSL) were reported less than ten years ago [1,2]. SBSL is a light emission phenomenon from a single bubble in liquid irradiated by an ultrasonic wave. The light is emitted at the collapse of the bubble. The pulse width of the light is experimentally measured to be less than 50 ps [3,4]. The spectrum is broadband and can be fitted by a black-body formula with the effective temperatures ranging from 6000 to 25 000 K [5–8]. The light pulse is emitted periodically with the frequency of the ultrasonic wave [4].

As the mechanism of light emission, it is widely suggested [1,9–17] that a spherically converging shock wave develops inside a bubble at the strong collapse and that gases are ionized when the shock converges at the center of the bubble and that the light is emitted by thermal bremsstrahlung in the plasma. However, Kordomenos, Bernard, and Denardo [18] observed no microwave from a SBSL bubble though it should be observed if the light is originated in thermal bremsstrahlung. Additionally, Weninger, Putterman, and Barber [19] reported the deviation from the sphericity about the shape of a SBSL bubble from the experimental observation of the angular correlation of the light. They reported that the ellipticity, which is defined as $(a/b-1)$ where a,b are the major, minor axes of a SBSL bubble, is sometimes 20%. This disagrees with the shock-wave theory because the accurate sphericity of the bubble is required in order to develop a spherical shock wave which converges at the center of the bubble. Vuong and Szeri [20] found by their numerical calculations of hydrodynamic equations including the effect of viscosity and thermal conduction in the gas inside the bubble that there is no sharp shock focusing at the bubble center for a noble gas bubble. Finally, Kwak and co-workers [21,22] found in their theoretical studies that almost the whole bubble is heated up at the collapse rather than a local point (the bubble center) being heated by a spherically converging shock wave. Kwak and co-workers [21,22] pointed out in their analytical calculations of the conservation laws of mass, momentum, and energy of gases inside the bubble that the temperature inside the bubble increases and decreases in a quite short time at the end of the strong collapse due to the sudden increase and decrease of the bubble wall acceleration ($\ddot{R}$, where R is the bubble radius and the dot denotes time derivative) at the time when the bubble wall velocity ($\dot{R}$) suddenly changes to zero. The importance of the bubble wall acceleration ($\ddot{R}$) is partly due to the change of the kinetic energy of gas inside the bubble into heat. This is seen as follows. The velocity profile of gases inside the bubble is [21]

$$v_g(r)=\frac{\dot{R}}{R}\,r, \tag{1}$$

where v_g is the velocity of gas inside the spherical bubble and r is the radius from the bubble center. Thus the total kinetic energy of gas inside the bubble ($K_{\rm tot}$) is

$$K_{\rm tot}=\int \frac{1}{2}\,v_g^2\rho dV=\frac{1}{2}\left(\frac{\dot{R}}{R}\right)^2\int_0^R \rho r^2 4\pi r^2 dr$$

$$\cong 2\pi\left(\frac{\dot{R}}{R}\right)^2\overline{\rho}\,\frac{R^5}{5}=\frac{3}{10}\,M\dot{R}^2, \tag{2}$$

where ρ is the density of gas inside the bubble and it is assumed that ρ is constant ($\overline{\rho}$) throughout the bubble. M is the total mass of the gas inside the bubble ($M=\frac{4}{3}\pi R^3\overline{\rho}$). Thus the change of the kinetic energy ($\Delta K_{\rm tot}$) in time Δt is proportional to $\ddot{R}$.

$$\Delta K_{\rm tot}=\frac{dK_{\rm tot}}{dt}\,\Delta t=\frac{3}{5}\,M\dot{R}\ddot{R}\Delta t. \tag{3}$$

When the kinetic energy of gas inside the bubble decreases (when $\Delta K_{\rm tot}<0$), the energy ($\Delta K_{\rm tot}$) changes to heat and the

temperature inside the bubble (T) increases. In other words, the kinetic energy of gas heats up the bubble when the gas stops their motion at the end of the strong collapse. This is one of the reasons for the strong dependence of the temperature inside the bubble (T) on the bubble wall acceleration ($\ddot{R}$) in the theoretical results by Kwak and Na [22]. In the present paper the temperature inside the bubble is assumed to be spatially uniform except at the thermal boundary layer near the bubble wall even at the strong collapse, based on the theoretical results of Kwak and Na [22] that spatial variation of temperature inside the bubble is less than a few tens of percent even at the final stage of the strong collapse. In the present paper, the effect of the kinetic energy of gas is taken into account in a different manner compared with that by Kwak and Na [22] (see the next section), which was neglected in the previous papers by the present author [23–26]. There are three important different points in the present paper compared with those by Kwak and co-workers [21,22]. One is the different formulation of bubble dynamics. In [21,22], the conservation equations of mass, momentum, and energy are analytically calculated. However, in their analysis, physical meanings of the resultant equations are unclear. In the present formulation, the physical meanings are much more easily understandable. The second point is that the argon bubble is studied in the present paper based on the hypothesis of Lohse *et al.* [27] as is described in detail later, while an air bubble is studied in [21,22]. The other point is that the effect of chemical reactions inside the bubble is taken into account in the present paper, while it is not in [21,22].

Next the hypothesis by Lohse *et al.* [27] is briefly reviewed. They suggested that a SBSL bubble in water containing air consists mainly of argon. By their hypothesis, the strange phenomena known in SBSL experiments [28–30] concerning mass diffusion are all explained clearly without introducing any exotic ideas. They assumed that nitrogen and oxygen molecules chemically react to be soluble species such as NO_x, HNO_x, OH at the strong collapses of the bubble and that they gradually dissolve into the surrounding water, which results in the bubble consisting mainly of argon that is chemically stable and that is not so easily soluble in water. Barber *et al.* [28] reported their experimental results that a SBSL bubble in water in which air is dissolved by 20% of the saturation repeats light emissions with accurate periodicity, which means that the mass diffusion is accurately balanced; the amount of gas (noncondensable gas) diffusing out of the bubble into water at the collapses is equal to that diffusing into the bubble from the surrounding water at the expansion (a bubble collapses a few times in one acoustic cycle [see Fig. 1(b)]). However, the classical Eller-Flynn theory [31] of mass diffusion fails to explain the above results because it predicts the gradual growth of the bubble under the experimental condition of the air concentration in water and the amplitude and the frequency of the ultrasonic wave. The hypothesis of Lohse *et al.* [27] explains this discrepancy because argon is dissolved in water by 0.2% of its saturation under the condition due to the fact that the percentage of argon in air is 1% and the Eller-Flynn theory predicts the stable balance of mass diffusion at the degree of saturation (0.2%). The hypothesis also explains the strange experimental results of Hiller *et al.* [29] that the oscillations of a nitrogen bubble in the acoustic field are dramatically stabilized by doping 1% of noble gas. The nitrogen bubble grows gradually under the experimental condition according to the Eller-Flynn theory in the time scale of 0.1–10 s while the acoustic period is on the order of 10^{-5} s. Finally the surface oscillations are strongly activated because the bubble is too big to be stably spherical and the bubble breaks up into tiny bubbles [30]. Some of the tiny bubbles recombine at the antinode of the standing acoustic wave toward which the radiation force (Bjerknes force) acts [32]. The combined bubble again grows gradually according to the Eller-Flynn theory and this history is repeated [30]; this is the mechanism of the unstable oscillations of pure nitrogen bubble that are observed [29]. When 1% noble gas is doped in the water, the physical situation is dramatically changed according to the hypothesis of Lohse *et al.* [27]. In this case, the bubble consists mainly of argon and the Eller-Flynn theory predicts the stable balance of mass diffusion concerning argon because the degree of saturation for argon is small enough [27]. Of course nitrogen also diffuses into the bubble at the expansion. However, they chemically react with vapor molecules (H_2O) to be soluble species at the collapse and they dissolve into the surrounding water. Lohse's hypothesis also explain clearly the experimental results of Holt and Gaitan [30] that the Eller-Flynn (EF) theory cannot explain the stability of the SBSL bubble in water containing air. They reported [30] that the SBSL bubble should gradually grow according to the EF theory and that the concentration of the gas in water should be 1% of the real one in order to explain the stability by EF theory. This contradiction is clearly dissolved by the hypothesis of Lohse *et al.* [27] because the concentration of argon in air is just 1%. As is seen above, the hypothesis [27] explains clearly the strange experimental results [28–30] of SBSL concerning mass diffusion. Thus in the present paper the bubble is assumed to consist of argon and water vapor, which results in higher temperature in a bubble at the collapse because the molar heat of argon (monoatomic molecules) is smaller than that of air (mostly diatomic molecules).

In the present paper, the effect of nonequilibrium evaporation and condensation of water vapor at the bubble wall, that of thermal conduction both inside and outside the bubble, and that of chemical reactions inside the bubble are taken into account. The purpose of the present paper is to investigate the thermal radiation mechanism from the whole bubble rather than a local point (the bubble center) heated by shock wave, which is motivated by the theoretical results of Kwak and co-workers [21,22] that the whole bubble is heated up at the final stage of the collapse.

II. MODEL

The physical situation is that of a single spherical bubble in water irradiated by an ultrasonic wave. The contents of the bubble are noncondensable gas (argon) and water vapor. In the present study, small amounts of chemical products also exist in the bubble as noncondensable gases. Pressure (p_g) inside a bubble is assumed to be spatially uniform. The temperature inside the bubble (T) is assumed to be spatially uniform except for a thin boundary layer near the bubble wall even at the collapse of the bubble, which is based on the

theoretical results of Kwak and Na [22]. The thickness of the boundary layer is assumed to be $n\lambda$ where n is a constant and λ is the mean free path of a gas molecule [23,33]. It is assumed that the temperature in the boundary layer changes linearly with radius (r): from T at $r=R-n\lambda$ to T_B at $r=R$, where R is the bubble radius and T_B is the gas temperature at the bubble wall [the origin of the radius (r) is the bubble center] [23]. Thus

$$\left.\frac{\partial T}{\partial r}\right|_{r=R}=\frac{T_B-T}{n\lambda}. \tag{4}$$

The mean free path (λ) is calculated by Eq. (5) [34].

$$\lambda=\frac{V}{\sqrt{2}\sigma' n_t}, \tag{5}$$

where σ' is the cross section of a molecule in the bubble (in this calculation, $\sigma'=0.4\times10^{-18}$ m^2 is employed).

As a well known result of the kinetic theory of gases, temperature jump (ΔT) exists at the bubble wall [35].

$$T_B=T_{L,i}+\Delta T, \tag{6}$$

where $T_{L,i}$ is the liquid temperature at the bubble wall. The temperature jump (ΔT) is given by Eq. (7) [35].

$$\Delta T=-\frac{1}{2kn'}\sqrt{\frac{\pi m}{2kT_B}}\frac{2-a'\alpha_e}{\alpha_e}\kappa\left.\frac{\partial T}{\partial r}\right|_{r=R}, \tag{7}$$

where k is the Boltzmann constant, n' is the number density of gas and vapor molecules in the bubble, m is the mean mass of a molecule, α_e is the thermal accommodation coefficient, a' is a constant ($a'=0.827$ [35]), and κ is the thermal conductivity of the gas.

The thermal conductivity (κ) is calculated by the following equation as a function of temperature [36].

$$\kappa=0.009+3.2\times10^{-5}T, \tag{8}$$

where κ is in W/m K and T is in K, which gives a reasonable representation of measured values over the range from 250 to 2000 K, which is the only one where data are available for argon [37].

In the model, the number of water molecules in the bubble (n_{H_2O}) changes with time due to evaporation or condensation at the bubble wall and chemical reactions.

$$n_{H_2O}(t+\Delta t)=n_{H_2O}(t)+4\pi R^2\dot{m}\Delta t+\tfrac{4}{3}\pi R^3\Delta t[\Sigma(\text{production})-\Sigma(\text{destruction})], \tag{9}$$

where t is the time, and $\dot{m}$ is the net rate of evaporation per unit area and unit time (when $\dot{m}<0$, condensation takes place). The first sum in the right hand side of Eq. (9) contains the contribution of all reactions producing H_2O, and the second one contains that of all the reactions consuming H_2O. Details of the chemical kinetics are described later. The rate of evaporation per unit area and unit time ($\dot{m}$) is calculated by Eqs. (10)–(12) [23–25,38,39].

$$\dot{m}=\dot{m}_{\text{eva}}-\dot{m}_{\text{con}}, \tag{10}$$

$$\dot{m}_{\text{eva}}=\frac{10^3N_A}{M_{H_2O}}\frac{\alpha_M}{(2\pi R_v)^{1/2}}\frac{p_v^*}{T_{L,i}^{1/2}}, \tag{11}$$

$$\dot{m}_{\text{con}}=\frac{10^3N_A}{M_{H_2O}}\frac{\alpha_M}{(2\pi R_v)^{1/2}}\frac{\Gamma p_v}{T_B^{1/2}}. \tag{12}$$

Equation (10) means that the net rate of evaporation ($\dot{m}$) is the difference between the actual rate of evaporation ($\dot{m}_{\text{eva}}$) and that of condensation ($\dot{m}_{\text{con}}$). In Eqs. (11) and (12), α_M is the accommodation coefficient for evaporation or condensation, R_v is the gas constant of water vapor in J/kg K, p_v^* is the saturated vapor pressure at temperature $T_{L,i}$, and p_v is the actual vapor pressure.

$$p_v=\frac{n_{H_2O}}{n_t}p_g. \tag{13}$$

The correction factor (Γ) in Eq. (12) is expressed as

$$\Gamma=\exp(-\Omega^2)-\Omega\sqrt{\pi}\left(1-\frac{2}{\sqrt{\pi}}\int_0^\Omega\exp(-x^2)dx\right) \tag{14}$$

in which

$$\Omega=\frac{\dot{m}}{p_v}\left(\frac{R_vT}{2}\right)^{1/2}. \tag{15}$$

The accommodation coefficient (α_M) is calculated as a function of liquid temperature by interpolating the results of molecular dynamics simulations by Matsumoto [40]. Details are described in the Appendix.

As the equation of bubble radius (R), Eq. (16) is employed, in which compressibility of liquid and the effect of evaporation and condensation of water vapor at the bubble wall are taken into account [the derivation of Eq. (16) is given in Ref. [24]]:

$$\begin{aligned}\left(1-\frac{\dot{R}}{c_\infty}+\frac{\dot{m}}{c_\infty\rho_{L,i}}\right)R\ddot{R}+\frac{3}{2}\dot{R}^2\left(1-\frac{\dot{R}}{3c_\infty}+\frac{2\dot{m}}{3c_\infty\rho_{L,i}}\right)&=\frac{1}{\rho_{L,\infty}}\left(1+\frac{\dot{R}}{c_\infty}\right)\left[p_B-p_s\left(t+\frac{R}{c_\infty}\right)-p_\infty\right]+\frac{\ddot{m}R}{\rho_{L,i}}\\&\times\left(1-\frac{\dot{R}}{c_\infty}+\frac{\dot{m}}{c_\infty\rho_{L,i}}\right)+\frac{\dot{m}}{\rho_{L,i}}\left(\dot{R}+\frac{\dot{m}}{2\rho_{L,i}}+\frac{\dot{m}\dot{R}}{2c_\infty\rho_{L,i}}\right.\\&\left.-\frac{R}{\rho_{L,i}}\frac{d\rho_{L,i}}{dt}-\frac{\dot{m}R}{c_\infty\rho_{L,i}^2}\frac{d\rho_{L,i}}{dt}\right)+\frac{R}{c_\infty\rho_{L,\infty}}\frac{dp_B}{dt},\end{aligned} \tag{16}$$

where the dot denotes the time derivative (d/dt), c_∞ is the sound speed in the liquid at infinity, $\rho_{L,i}$ ($\rho_{L,\infty}$) is the liquid density at the bubble wall (at infinity), $p_B(t)$ is the liquid pressure on the external side of the bubble wall, $p_s(t)$ is a nonconstant ambient pressure component such as a sound field, and p_∞ is the undisturbed pressure. $p_B(t)$ is related to the pressure inside the bubble [$p_g(t)$] by Eq. (17) [24,39]:

$$p_B(t)=p_g(t)-\frac{2\sigma}{R}-\frac{4\mu}{R}\left(\dot{R}-\frac{\dot{m}}{\rho_{L,i}}\right)-\dot{m}^2\left(\frac{1}{\rho_{L,i}}-\frac{1}{\rho_g}\right), \tag{17}$$

where σ is the surface tension, μ is the liquid viscosity, and ρ_g is the density inside the bubble. When a bubble is irradiated by an acoustic wave the wavelength of which is much larger than the bubble radius, $p_s(t)=-A\sin\omega t$ where A is the pressure amplitude of the acoustic wave and ω is its angular frequency.

In order to calculate $p_g(t)$, the van der Waals equation of state is employed.

$$\left(p_g(t)+\frac{a}{v^2}\right)(v-b)=R_gT, \tag{18}$$

where a and b are the van der Waals constants, v is the molar volume, R_g is the gas constant, and T is the temperature inside the bubble. In this model, the van der Waals constants (a and b) change with time due to the change of n_{H_2O} [41].

$$a=a_{Ar}\left(\frac{n_{Ar}}{n_t}\right)^2+2a_{Ar\text{-}H_2O}\left(\frac{n_{Ar}}{n_t}\right)\left(\frac{n_{H_2O}}{n_t}\right)+a_{H_2O}\left(\frac{n_{H_2O}}{n_t}\right)^2, \tag{19}$$

$$b=b_{Ar}\left(\frac{n_{Ar}}{n_t}\right)^2+2b_{Ar\text{-}H_2O}\left(\frac{n_{Ar}}{n_t}\right)\left(\frac{n_{H_2O}}{n_t}\right)+b_{H_2O}\left(\frac{n_{H_2O}}{n_t}\right)^2, \tag{20}$$

where a_{Ar} and b_{Ar} (a_{H_2O} and b_{H_2O}) are the van der Waals constants of argon (water vapor), $a_{Ar\text{-}H_2O}=\sqrt{a_{Ar}a_{H_2O}}$, $\sqrt[3]{b_{Ar\text{-}H_2O}}=\frac{1}{2}\left(\sqrt[3]{b_{Ar}}+\sqrt[3]{b_{H_2O}}\right)$ [41]. The values are as follows [34]: $a_{Ar}=1.345\times10^{-1}$ J m^3/mol^2, $a_{H_2O}=5.536\times10^{-1}$ J m^3/mol^2, $b_{Ar}=3.219\times10^{-5}$ m^3/mol, $b_{H_2O}=3.049\times10^{-5}$ m^3/mol. In the present calculations, the effect of the chemical products on the van der Waals constants is neglected, because the amount of the chemical products is small, as seen in the next section.

The temperature inside the bubble (T) is calculated by solving Eq. (21).

$$E=\frac{n_{Ar}}{N_A}C_{V,Ar}T+\frac{n_{H_2O}}{N_A}C_{V,H_2O}T+\frac{T}{N_A}\sum_\alpha n_\alpha C_{V,\alpha}-\left(\frac{n_t}{N_A}\right)^2\frac{a}{V}, \tag{21}$$

where E is the thermal energy of the bubble, n_t is the total number of gas and vapor molecules in the bubble, V is the volume of the bubble, $C_{V,Ar}$(C_{V,H_2O}) is the molar heat of argon (vapor) at constant volume, α denotes species of the chemical products such as OH, O_2, O_3, HO_2, H_2O_2, H_2, H, and O, and the summation is for all the chemical products considered here. The molar heat is assumed as follows; for monoatomic gases such as Ar, H, and O, the molar heat is $\frac{3}{2}R_g$, for diatomic gases such as OH, O_2, and H_2, it is $\frac{5}{2}R_g$, for the other gases, it is $\frac{6}{2}R_g$ [42].

The change of the thermal energy of a bubble (ΔE) in time Δt is expressed by

$$\Delta E(t)=-p_g(t)\Delta V(t)+4\pi R^2\dot{m}e_{H_2O}\Delta t+4\pi R^2\kappa\left.\frac{\partial T}{\partial r}\right|_{r=R}\Delta t+\frac{4}{3}\pi R^3\Delta t\sum_r(r_{\gamma b}-r_{\gamma f})\Delta H_{\gamma f}+\left[-\frac{3}{5}M\dot{R}\ddot{R}\right]\Delta t, \tag{22}$$

where e_{H_2O} is the energy carried by an evaporating or condensing vapor molecule, $r_{\gamma f}$($r_{\gamma b}$) is the forward (backward) reaction rate of the reaction γ per unit volume and unit time, $\Delta H_{\gamma f}$ is the enthalpy change in the forward reaction (when $\Delta H_{\gamma f}<0$, the reaction is exothermic), and M is the total mass of gases and vapor inside the bubble. The first term in the right hand side of Eq. (22) is the work by pressure (pV work). The second term is the energy carried by evaporating or condensing vapor molecules. The third term is the energy change due to thermal conduction. The fourth term is the heat of chemical reactions inside the bubble. The last term is the effect of the kinetic energy of gas described in the preceding section [Eq. (3)]. The brackets mean that this term is included only when the term is positive, which corresponds to the decrease of the kinetic energy. When the term is negative, it is replaced by zero.

The energy carried by an evaporating or condensing vapor molecule e_{H_2O} is calculated by Eq. (23) [26].

$$e_{H_2O}=\frac{C_{V,H_2O}}{N_A}T_B. \tag{23}$$

Following is the description of the variation of liquid temperature at the bubble wall [24]. Continuity of energy flux at the bubble wall is given by Eq. (24).

$$\kappa_L\left.\frac{\partial T_L}{\partial r}\right|_{r=R}=\kappa\left.\frac{\partial T}{\partial r}\right|_{r=R}+\dot{m}L+\frac{\dot{m}}{N_A}C_{V,H_2O}(T_B-T_{L,i}), \tag{24}$$

where κ_L is the thermal conductivity of liquid water, $T_L(r)$ is the liquid temperature at radius r, and L is the latent heat of evaporation or condensation. κ_L and L depend on the liquid temperature and the liquid pressure. Their formulas are described in Ref. [24]. In this model, $(\partial T_L/\partial r)|_{r=R}$ is calculated by Eq. (24).

The spatial distribution of the liquid temperature [$T_L=T_L(r)$] should satisfy the following boundary conditions:

$$T_L(R)=T_{L,i}, \tag{25}$$

$$\left.\frac{\partial T_L(r)}{\partial r}\right|_{r=R}=\left.\frac{\partial T_L}{\partial r}\right|_{r=R}, \tag{26}$$

$$T_L(r\to\infty)=T_\infty, \tag{27}$$

$$\left.\frac{\partial T_L(r)}{\partial r}\right|_{r\to\infty}=0, \tag{28}$$

where T_∞ is the ambient liquid temperature. In the present model, the temperature profile in the liquid is assumed to be exponential [Eqs. (29) and (30)].

When

$$(T_{L,i}-T_\infty)\left.\frac{\partial T_L}{\partial r}\right|_{r=R}<0, \tag{29}$$

$$T_L(r)=(T_{L,i}-T_\infty)\exp\left(-\frac{\left.\frac{\partial T_L}{\partial r}\right|_{r=R}}{(T_\infty-T_{L,i})}(r-R)\right)+T_\infty .$$

When

$$(T_{L,i}-T_\infty)\left.\frac{\partial T_L}{\partial r}\right|_{r=R}>0, \tag{30}$$

$$T_L(r)=A\ \exp[-B(r-C)^2]+T_\infty ,$$

where

$$A=(T_{L,i}-T_\infty)\exp(Be_1^2),$$

$$B=\frac{\left.\frac{\partial T_L}{\partial r}\right|_{r=R}}{2(T_{L,i}-T_\infty)}\frac{1}{e_1},$$

$$C=R+e_1,$$

$$e_1=e_0\left|\frac{T_{L,i}-T_B}{\left.\frac{\partial T_L}{\partial r}\right|_{r=R}}\right|,$$

where e_0 is a parameter which was determined to fit the calculated results of the radius-time curve with the experimental data by Barber and Putterman [43] in the previous paper by the presant author [24]. The value is $e_0=1\times10^{-3}$ [24]. Both Eqs. (29) and (30) satisfy the boundary conditions [Eqs. (25)–(28)].

In the present model, a boundary layer is assumed in liquid phase near a bubble. The thickness of the layer (δ_L) is assumed as Eqs. (31) and (32).

When

$$(T_{L,i}-T_\infty)\left.\frac{\partial T_L}{\partial r}\right|_{r=R}<0, \tag{31}$$

$$\delta_L=\frac{T_\infty-T_{L,i}}{\left.\frac{\partial T_L}{\partial r}\right|_{r=R}}.$$

When

$$(T_{L,i}-T_\infty)\left.\frac{\partial T_L}{\partial r}\right|_{r=R}>0, \tag{32}$$

$$\delta_L=\frac{1}{\sqrt{B}}+e_1 .$$

Variation of the liquid temperature at the bubble wall ($T_{L,i}$) is calculated by Eq. (33).

$$T_{L,i}(t+\Delta t)=T_{L,i}(t)+\frac{4\pi R^2 j_1\Delta t-4\pi(R+\delta_L)^2 j_2\Delta t}{\frac{4}{3}\pi[(R+\delta_L)^3-R^3]\rho_{L,i}c_p}, \tag{33}$$

where $j_1(j_2)$ is the energy flux at $r=R(r=R+\delta_L)$ per unit area and unit time, and c_p is the specific heat of liquid water at constant pressure. j_1 and j_2 are calculated by Eqs. (34) and (35).

$$j_1=-\kappa_L|_{r=R}\left.\frac{\partial T_L}{\partial r}\right|_{r=R}, \tag{34}$$

$$j_2=-\kappa_L|_{r=R+\delta_L}\left.\frac{\partial T_L}{\partial r}\right|_{r=R+\delta_L}. \tag{35}$$

The assumed profile of liquid temperature [Eqs. (29) and (30)] is used only in the calculation of j_2 in Eq. (35).

Physical quantities of liquid depend on the liquid temperature and the liquid pressure. Formulas of the quantities employed in the calculations are described in Ref. [24].

Following is the description of the chemical kinetics. In Table I the chemical kinetic model [36,44] used in the present calculations is shown. The scheme of Table I has been partially validated by hydrogen frame studies [36]. Here we consider a simple reaction (γ),

$$aA+bB\rightarrow mM+nN,$$

where a,b and m,n are the number of molecules contributing to one reaction (γ) of the species A,B and M,N, respectively. The forward reaction rate per unit volume and unit time ($r_{\gamma f}$) is calculated from [36,44]

$$r_{\gamma f}=k_{\gamma f}[A]^a[B]^b, \tag{36}$$

where

$$k_{\gamma f}=A_{\gamma f}T^{\beta_{\gamma f}}\exp(-C_{\gamma f}/T), \tag{37}$$

where $A_{\gamma f}$, $\beta_{\gamma f}$, and $C_{\gamma f}$ are given in Table I. $[A]$ is the concentration of the species A. The backward reaction rate per unit volume and unit time ($r_{\gamma b}$) is calculated in the same manner.

$$r_{\gamma b}=k_{\gamma b}[M]^m[N]^n, \tag{38}$$

where

$$k_{\gamma b}=A_{\gamma b}T^{\beta_{\gamma b}}\exp(-C_{\gamma b}/T), \tag{39}$$

where $A_{\gamma b}$, $\beta_{\gamma b}$, and $C_{\gamma b}$ are given in Table I.

The number of each species (n_α) changes with time due to chemical reactions. (As described above, for H_2O, the number of molecules changes mainly by evaporation or condensation.)

$$n_\alpha(t+\Delta t)=n_\alpha(t)+\tfrac{4}{3}\pi R^3\Delta t[\Sigma(\text{production})-\Sigma(\text{destruction})], \tag{40}$$

TABLE I. The chemical kinetic model used in the calculations [36,44]. The concentrations of each species are expressed in moles per m^3. [Thus A_f (or A_b) is expressed in m^3/mol s for a two-body reaction (in m^6/mol^2 s for a three-body reaction).] β is dimensionless, and C is in K. For some of the backward reactions, the constants are not listed. Those backward reactions are neglected in the present calculations. ΔH_f is the enthalpy change in the forward reaction in kJ/mol at 1 atm and 1000 K. When $\Delta H_f < 0$, the forward reaction is exothermic.

No.	Reaction	A_f	β_f	C_f (K)	A_b	β_b	C_b (K)	ΔH_f (kJ/mol)
1	$H+O_2 \rightarrow O+OH$	1.92×10^{8}	0	8270	7.18×10^{5}	0.36	−342	69.17
2	$O+H_2 \rightarrow H+OH$	5.08×10^{-2}	2.67	3166	2.64×10^{-2}	2.65	2245	8.23
3	$OH+H_2 \rightarrow H+H_2O$	2.18×10^{2}	1.51	1726	1.02×10^{3}	1.51	9370	−64.35
4	$OH+OH \rightarrow H_2O+O$	2.1×10^{2}	1.4	200	2.21×10^{3}	1.4	8368	−72.59
5	$H_2+M \rightarrow H+H+M$ Coef. H_2:2.5, H_2O:16.0	4.58×10^{13}	−1.4	52500	2.45×10^{8}	−1.78	480	444.47
6	$O+O+M \rightarrow O_2+M$ Coef. H_2:2.5, H_2O:16.0	6.17×10^{3}	−0.5	0	1.58×10^{11}	−0.5	59472	−505.40
7	$O+H+M \rightarrow OH+M$ Coef. H_2O:5.0	4.72×10^{5}	−1.0	0	4.66×10^{11}	−0.65	51200	−436.23
8	$H+OH+M \rightarrow H_2O+M$ Coef. H_2:2.5, H_2O:16.0	2.25×10^{10}	−2.0	0	1.96×10^{16}	−1.62	59700	−508.82
9	$H+O_2+M \rightarrow HO_2+M$ Coef. H_2:2.5, H_2O:16.0	2.00×10^{3}	0	−500	2.46×10^{9}	0	24300	−204.80
10	$HO_2+H \rightarrow H_2+O_2$	6.63×10^{7}	0	1070	2.19×10^{7}	0.28	28390	−239.67
11	$HO_2+H \rightarrow OH+OH$	1.69×10^{8}	0	440	1.08×10^{5}	0.61	18230	−162.26
12	$HO_2+O \rightarrow OH+O_2$	1.81×10^{7}	0	−200	3.1×10^{6}	0.26	26083	−231.85
13	$HO_2+OH \rightarrow H_2O+O_2$	1.45×10^{10}	−1.0	0	2.18×10^{10}	−0.72	34813	−304.44
14	$HO_2+HO_2 \rightarrow H_2O_2+O_2$	3.0×10^{6}	0	700	4.53×10^{8}	−0.39	19700	−175.35
15	$H_2O_2+M \rightarrow OH+OH+M$ Coef. H_2:2.5, H_2O:16.0	1.2×10^{11}	0	22900	9.0×10^{-1}	0.90	−3050	217.89
16	$H_2O_2+H \rightarrow H_2O+OH$	3.2×10^{8}	0	4510	1.14×10^{3}	1.36	38180	−290.93
17	$H_2O_2+H \rightarrow H_2+HO_2$	4.82×10^{7}	0	4000	1.41×10^{5}	0.66	12320	−64.32
18	$H_2O_2+O \rightarrow OH+HO_2$	9.55	2	2000	4.62×10^{-3}	2.75	9277	−56.08
19	$H_2O_2+OH \rightarrow H_2O+HO_2$	1.00×10^{7}	0	900	2.8×10^{7}	0	16500	−128.67
20	$O_3+M \rightarrow O_2+O+M$	2.48×10^{8}	0	11430	4.1	0	−1057	109.27
		Coef. O_2:1.64			Coef. O_2:1.63, H_2O:15			
21	$O_3+O \rightarrow O_2+O_2$	5.2×10^{6}	0	2090				−396.14
22	$O_3+OH \rightarrow O_2+HO_2$	7.8×10^{5}	0	960				−164.95
23	$O_3+HO_2 \rightarrow O_2+O_2+OH$	1×10^{5}	0	1410				−121.92
24	$H+O_3 \rightarrow HO_2+O$	9×10^{6}	0.5	2010				135.65
25	$H+O_3 \rightarrow OH+O_2$	1.6×10^{7}	0	0				−96.20

where the first sum on the right hand side of Eq. (40) contains the contribution of all reactions producing α, and the second one contains that of all reactions consuming α. For example, when $\alpha = A$ in the reaction (γ), $ar_{\gamma f}$ contributes to the second sum in Eq. (40) (in this stage, $ar_{\gamma f}$ should be expressed in molecules/m^3 s). In Table I, M denotes the collision partner or the third body in a three-body reaction, which acts only as catalyst in the reaction. The listed values in Table I are those for $M = \mathrm{Ar}$. In case of the other species ($M \neq \mathrm{Ar}$), the value $A_{\gamma f}$ (or $A_{\gamma b}$) for $M = \mathrm{Ar}$ should be multiplied by the coefficient listed in the table. For unlisted species, the value $A_{\gamma f}$ (or $A_{\gamma b}$) for $M = \mathrm{Ar}$ is employed in the present calculations.

III. RESULTS AND DISCUSSIONS

Calculations are performed under a condition of SBSL [30]. The initial bubble radius is 5 μm [30]. The frequency and the amplitude of acoustic wave are 20.6 kHz and 1.35 bars, respectively [30]. The ambient liquid temperature (T_∞) and the ambient pressure (p_∞) are chosen to be 20 °C and 1 atm, respectively. The initial number of chemical products (n_α) is chosen to be zero ($n_\alpha = 0$). As in the calculations in Refs. [23–26,33], $n = 3$ is assumed, which determines the thickness of the thermal boundary layer inside a bubble ($n\lambda$). α_e in Eq. (7) is assumed to be $\alpha_e = 1.0$ [39].

Calculated results for one acoustic cycle (0–48.5 μs) are shown in Figs. 1(b)–1(f). In Fig. 1(a), the acoustic field [$p_s(t)$] applied on the bubble is shown as a function of time. The time axes in Figs. 1(a)–1(f) are the same. In Fig. 1(b), the bubble radius (R) is shown as a function of time. It is seen that the bubble expands when the acoustic pressure (p_s) is negative and that it collapses strongly when p_s becomes positive. After the strongest collapse, it oscillates softly a few times with its own frequency [32]. In Fig. 1(c), the pressure inside the bubble (p_g) is shown as a function of time with logarithmic vertical axis. It is seen that p_g increases up to 10 GPa at the strongest collapse and that soft oscillations follow due to the soft oscillations of the bubble radius. In Fig. 1(d), the temperature inside a bubble (T) is shown as a function of time with logarithmic vertical axis. It is seen that the expansion of the bubble is the isothermal process while

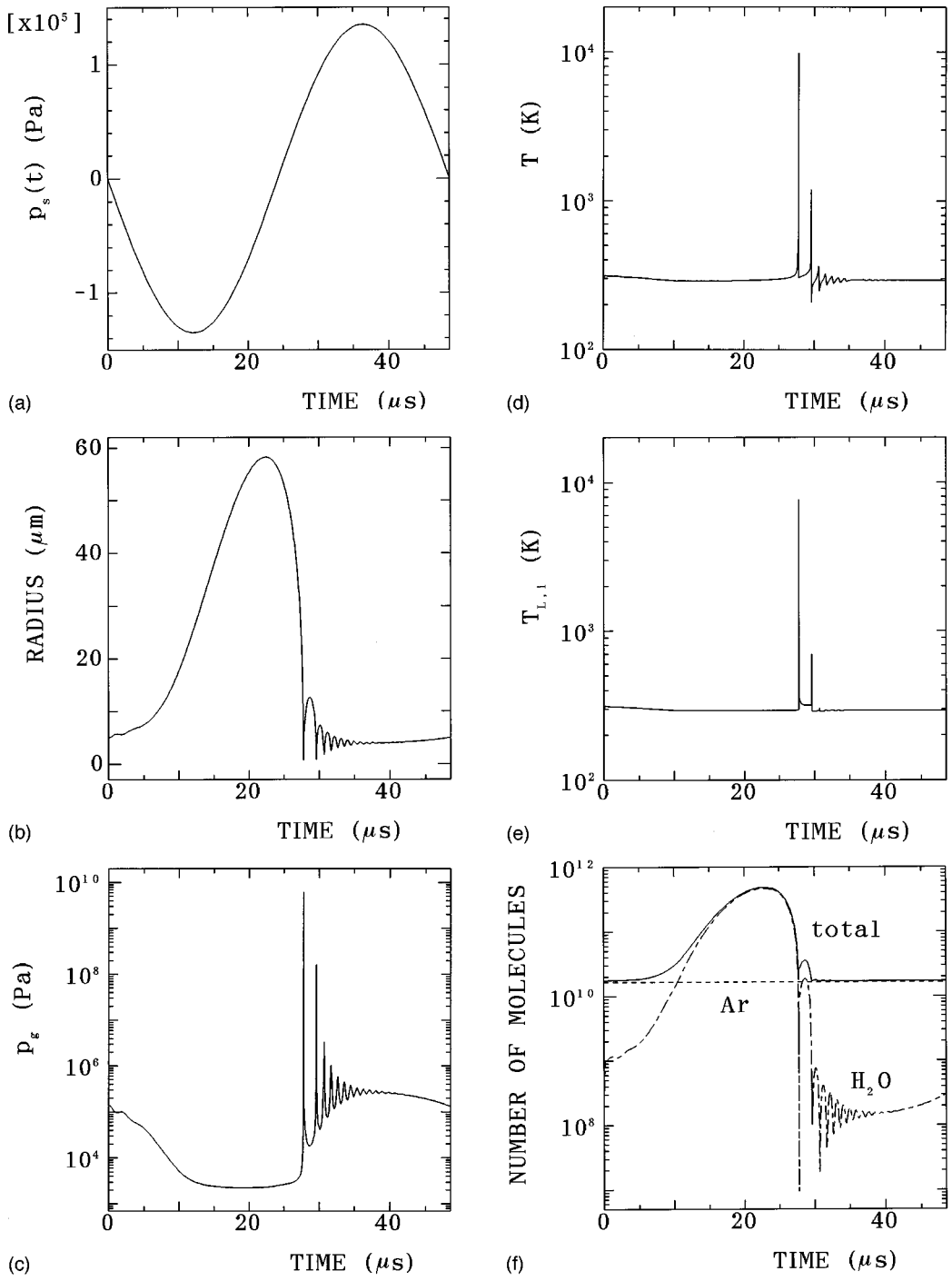

FIG. 1. Calculated results under the condition of SBSL [30] for one acoustic cycle. The time axes (the horizontal axes) are the same for all the figures. (a) The pressure of the acoustic field [$p_s(t)$] employed in the calculation. (b) The bubble radius (R). (c) The pressure inside the bubble (p_g) with logarithmic vertical axis. (d) The temperature inside the bubble (T) with logarithmic vertical axis. (e) The liquid temperature at bubble wall ($T_{L,i}$) with the same logarithmic vertical axis with that in (d). (f) The number of molecules in the bubble with logarithmic vertical axis. The line shows the total number of molecules in the bubble (n_t), the dotted line is the number of argon molecules (n_{Ar}), and the dash-dotted line is that of vapor molecules ($n_{\mathrm{H_2O}}$).

the collapses are rather adiabatic ones. It is seen that the temperature increases up to 10 000 K at the strongest collapse. In Fig. 1(e), the liquid temperature at the bubble wall ($T_{L,i}$) is shown as a function of time with the same logarithmic vertical axis with that in Fig. 1(d). It is seen that $T_{L,i}$ is identical to the ambient liquid temperature (T_∞) except at the two strong collapses. At the strongest collapse, $T_{L,i}$ increases dramatically up to the same order of magnitude with the temperature inside the bubble (T). This means that chemical reactions take place not only inside a bubble but also outside it as was clarified in the previous study by the present author [24] under a different physical condition. The heated liquid layer is very thin, on the order of 0.01 μm, for the region where the temperature is above 500 K [δ_L defined in Eq. (31) is 0.004 μm]. In Fig. 1(f), the number of molecules inside a bubble is shown as a function of time with logarithmic ver-

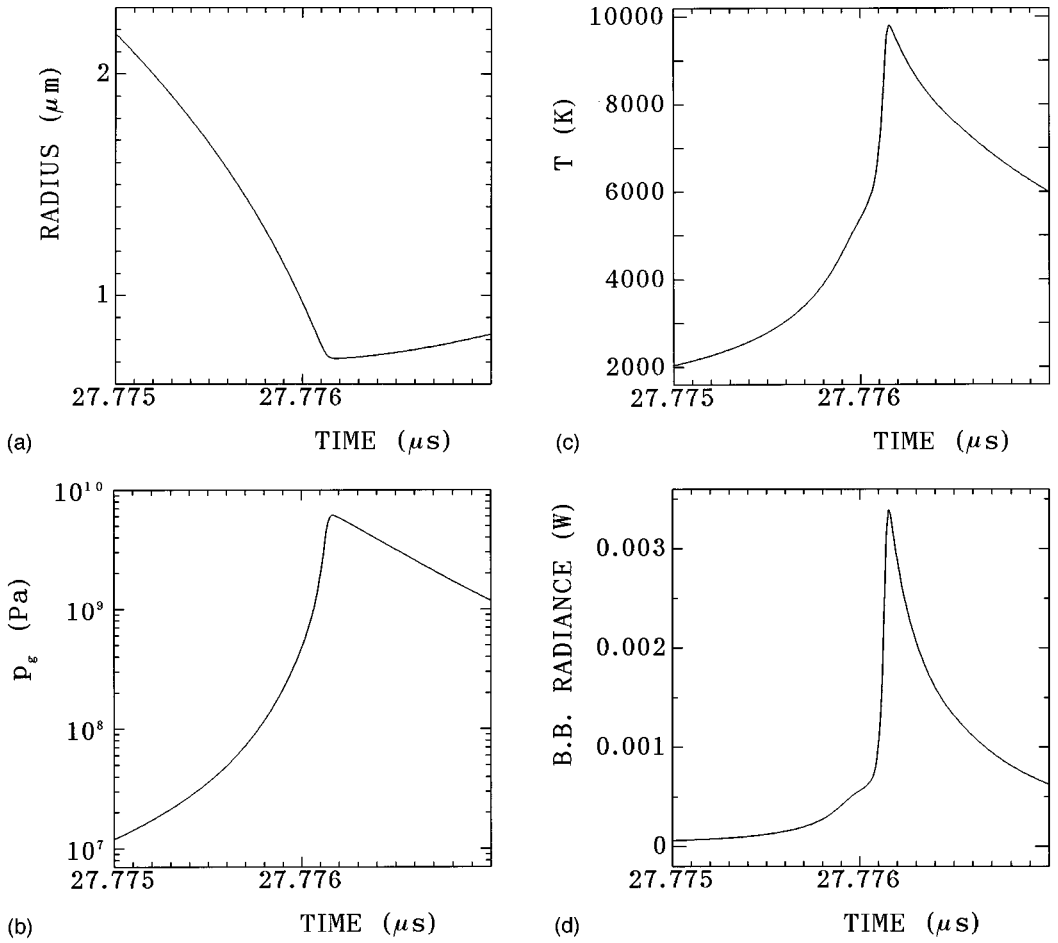

FIG. 2. Calculated results at around the minimum bubble radius as a function of time for 2000 ps (0.002 us). The time axes are the same throughout the figures. (a) The bubble radius (R). (b) The pressure inside the bubble (p_g) with logarithmic vertical axis. (c) The temperature inside the bubble (T). (d) The blackbody radiance (r_r). (e) The number of molecules inside the bubble with logarithmic vertical axis. The vertical axes are the same and the solid line is the total number of molecules (n_t) throughout (e)–(h). The dash-dotted line is the number of vapor molecules (n_{H_2O}), the dotted line is that of argon molecules (n_{Ar}), and the dashed line is that of OH radicals. (f) The number of O molecules (dotted line), that of O_2 molecules (dashed line), and that of O_3 molecules (dash-dotted line) inside the bubble. (g) The number of H molecules (dotted line) and that of H_2 molecules (dash-dotted line) inside the bubble. (h) The number of HO_2 molecules (dotted line) and that of H_2O_2 molecules (dash-dotted line) inside the bubble.

tical axis. The solid line is the total number of molecules. The dotted line and the dash-dotted line are the number of argon molecules and that of water molecules (vapor) inside the bubble, respectively. It is seen that the number of vapor molecules changes dramatically due to evaporation and condensation. It is seen that evaporation takes place at the expansion of the bubble because the pressure inside the bubble is low and that condensation takes place at the collapses because the pressure inside the bubble is high.

In Figs. 2(a)–2(h), the calculated results at around the minimum bubble radius are shown as a function of time for 2000 ps (0.002 μs). The time axes are the same throughout Figs. 2(a)–2(h). In Fig. 2(a), the bubble radius (R) is shown. It is seen that the strong collapse stops suddenly due to the sudden increase of pressure inside the bubble (p_g) shown in Fig. 2(b). The pressure increases three orders of magnitude in the last 1000 ps of the collapse and the time derivative of the pressure is very large, especially at the minimum bubble radius. It is because the strong collapse is ended when all the molecules in the bubble undergo van der Waals hard core collisions. As is seen in Fig. 2(a), the bubble wall velocity ($|R|$) increases up to 1900 m/s, which is larger than the sound velocity of gas inside the bubble at the time ($c_g = 1500$ m/s), which is calculated by

$$c_g = \left(\frac{dp_g}{d\rho_g}\right)^{1/2} = \left[\left(-\frac{R_g T}{(v-b)^2} + \frac{2a}{v^3}\right)\frac{dv}{d\rho_g}\right]^{1/2}, \tag{41}$$

$$\frac{dv}{d\rho_g} = -\frac{v^2}{[M_{H_2O}(n_{H_2O}/n_t) + M_{Ar}(n_{Ar}/n_t)]\times 10^{-3}}, \tag{42}$$

where ρ_g is the density inside the bubble. Thus the assumption of the spatial uniformity of pressure inside the bubble is out of order at this strongest collapse. Thus the calculated results at around the minimum bubble radius are not accurate in a quantitative sense. Nevertheless, the qualitative conclusions in the present paper are correct because the spatial variation of pressure inside the bubble at the strong collapse is not so large (a few tens of percent) according to the theoretical results by Kwak and co-workers [21,22].

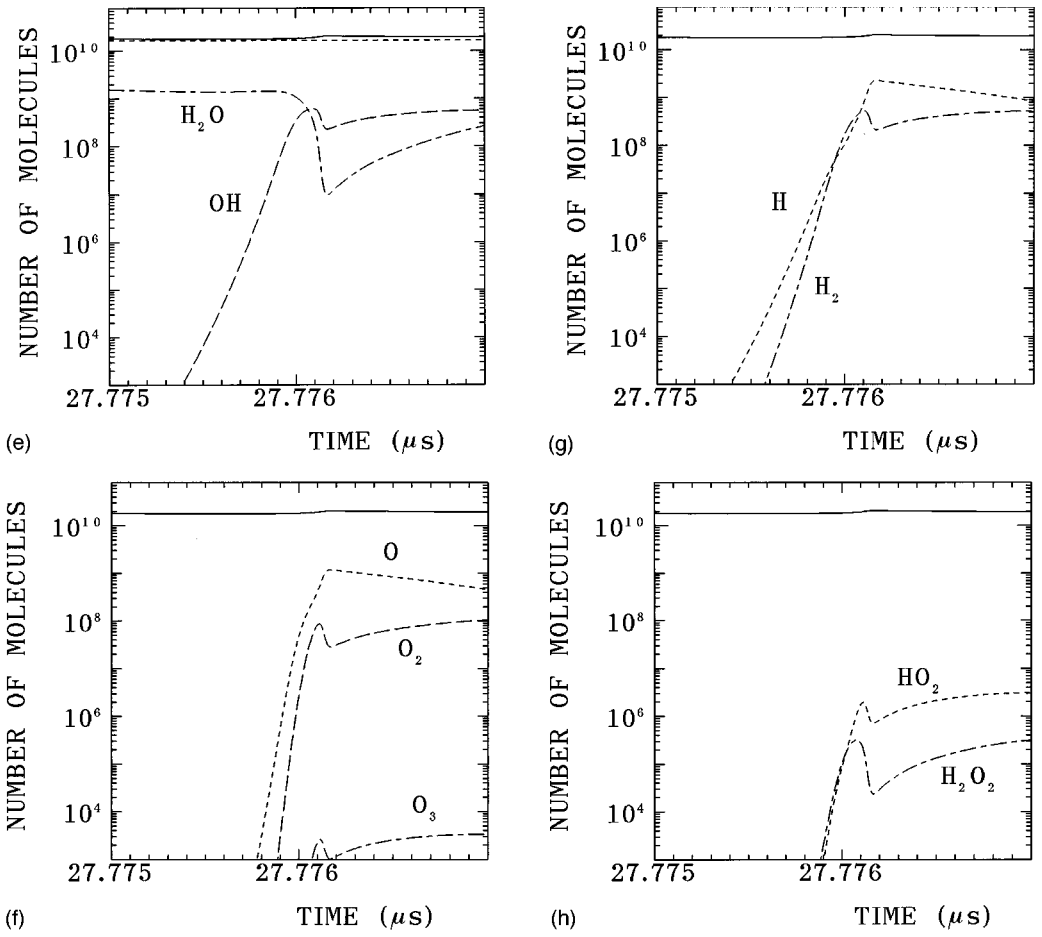

FIG. 2. (Continued)

In Fig. 2(c), the temperature inside the bubble (T) is shown. It is seen that T increases from 2000 to 10 000 K in the last 1000 ps (0.001 μs) of the collapse. Numerical results reveal that T increases from 6000 to 10 000 K in the last 120 ps (0.000 12 μs) of the collapse and that it is due to both pV work by the surrounding liquid and the effect of the kinetic energy of gases inside the bubble. In the last 120 ps, the increase of the thermal energy of the bubble by pV work is 2.3×10^{-9} J, while that by the effect of the kinetic energy is 1.3×10^{-9} J. It means that the kinetic energy of gases heats up the bubble considerably at the end of the collapse. In the last 120 ps, the thermal energy inside the bubble is reduced by 1.4×10^{-9} J by chemical reactions and by 0.6×10^{-9} J by thermal conduction. The reduction by the thermal radiation (blackbody radiation) is negligible (0.0002×10^{-9} J). Thus the net increase of the thermal energy inside the bubble is 1.7×10^{-9} J in the last 120 ps of the collapse. It is clarified that the thermal energy of the bubble is reduced considerably by endothermal chemical reactions. The chemical reactions decrease the temperature inside the bubble considerably due to the following two reasons; the reduction of the thermal energy by endothermal reactions and the increase of the number of molecules due to the dissociations of water (vapor) molecules. It is concluded that the effect of chemical reactions should be taken into account in the estimation of the temperatue inside the bubble at the strong collapse. In Fig. 2(d), the blackbody radiance is shown, which is calculated by the Stefan-Boltzmann law of radiation.

$$r_r=\frac{\pi^2k^4}{60c^2\hbar^3}\,T^4\times4\pi R^2, \tag{43}$$

where r_r is the blackbody radiance, k is the Boltzmann constant, c is the light velocity, and $\hbar=h/2\pi$ where h is the Planck constant. The half-width of the blackbody radiance is 250 ps, which is slightly larger than the experimentally observed pulse width of SBSL (50 ps) [4]. However, the total energy emitted in one pulse by the blackbody radiation is calculated to be 3 pJ ($=3\times10^{-12}$ J), while the experimentally measured value is 0.1–0.5 pJ [45] though the physical conditions are a little bit different. It means that the thermal radiation (blackbody radiation) is enough to account for the light emission of SBSL. In other words, the thermal radiation from the whole bubble cannot be neglected under the condition of SBSL. However, the thermal equilibrium of radiation with materials (gases) is assumed in the Stefan-Boltzmann law of radiation [Eq. (43)]. This assumption may be invalid in such a short time scale as 50 ps [4]. Thus for further discussions the nonequilibrium radiation field should be studied precisely. In the present study, the temperature is assumed to be spatially uniform inside a bubble except at the boundary layer near the bubble wall though the numerical results of Kwak and Na [22] show a slight spatial variation of temperature inside a bubble in the order of a few tens of percent. It is possible that the temperature near the bubble center is a few tens of percent higher than the calculated

temperature in the present study (it is a completely different situation from that of the shock-wave theory because in that case the difference of temperature between the center and the surrounding region is a few orders of magnitude). The higher temperature attained near the bubble center shortens the half-width of the thermal radiance because dr_r/dT is proportional to T^3 [see Eq. (43)]; at higher temperature the change of the radiance with unit temperature is larger. The higher temperature near the bubble center also increases the value of radiance itself because it is proportional to T^4 [Eq. (43)]. From these considerations, it is suggested that SBSL originates in the thermal radiation (or quasithermal radiation, which means the radiation at quasithermal equilibrium) from the whole bubble rather than the local point (the bubble center) suggested by the shock-wave theory [9–15].

In Figs. 2(e)–2(h), the numbers of molecules inside the bubble are shown with the same logarithmic vertical axes. The solid line shows the total number of molecules inside the bubble (n_t) throughout Figs. 2(e)–2(h). From Fig. 2(e), it is seen that almost all the water molecules (H_2O) undergo chemical reactions at the strong collapse because of the high pressure and temperature shown in Figs. 2(b) and 2(c). It is seen from Figs. 2(e)–2(h) that appreciable amounts of OH, O, O_2, O_3, H, H_2, HO_2, and H_2O_2 molecules are created inside the bubble at the strong collapse.

IV. CONCLUSION

A model of single-bubble sonoluminescence is constructed. In the model, the temperature is assumed to be spatially uniform inside the bubble except at the thermal boundary layer near the bubble wall even at the strong collapse based on the theoretical results of Kwak and co-workers [21,22] that the whole bubble is heated up rather than a local point (the bubble center) by the converging spherical shock wave suggested by the previous theories [9–15] of SBSL. In the present model, the effect of the kinetic energy of gases inside the bubble is taken into account, which changes to heat when the gases stop their motions at the end of the strong collapse, in a different manner from that in [21,22]. In the model, a bubble is assumed to consist mainly of argon based on the hypothesis by Lohse *et al.* [27]. Numerical calculations under a condition of SBSL reveal that the kinetic energy of gases heats up the bubble considerably at the final stage of the strong collapse. It is also clarified that almost all the water vapor molecules undergo chemical reactions at the strong collapse, which decreases the temperature inside the bubble considerably due to the endothermal nature of the reactions and the increase of the number of molecules inside the bubble. It is suggested that SBSL originates in the thermal radiation (or quasithermal radiation) from the whole bubble rather than a local point (the bubble center) by a converging spherical shock wave suggested widely in the previous studies [9–15] of SBSL.

APPENDIX: THE ACCOMMODATION COEFFICIENT FOR EVAPORATION (α_M)

The accommodation coefficient (α_M) for evaporation or condensation of water vapor is calculated as a function of liquid temperature at bubble wall ($T_{L,i}$) by interpolating the results of molecular dynamics simulations by Matsumoto [40] by the Gregory-Newton formula of interpolation [46].

$$\alpha_M = 0.35 - 0.05k^{(1)} - 0.05k^{(2)} + 0.025k^{(3)},$$

where $k=[T_{L,i}(K)/50]-7$, $k^{(m)}=k(k-1)\cdots[k-(m-1)]$. The equation is valid only when $350\ \mathrm{K} \leqslant T_{L,i} \leqslant 500\ \mathrm{K}$. The value ($\alpha_M$) above 500 K (below 350 K) is assumed to be that at 500 K (350 K) in the present calculations.

[1] L. A. Crum, Phys. Today **47(9)**, 22 (1994).
[2] D. F. Gaitan, L. A. Crum, C. C. Church, and R. A. Roy, J. Acoust. Soc. Am. **91**, 3166 (1992).
[3] B. P. Barber and S. J. Putterman, Nature (London) **352**, 318 (1991).
[4] B. P. Barber, R. Hiller, K. Arisaka, H. Fetterman, and S. Putterman, J. Acoust. Soc. Am. **91**, 3061 (1992).
[5] R. Hiller, S. J. Putterman, and B. P. Barber, Phys. Rev. Lett. **69**, 1182 (1992).
[6] R. Hiller and S. J. Putterman, Phys. Rev. Lett. **75**, 3549 (1995); **77**, 2345 (1996).
[7] R. Hiller, Ph.D. thesis, University of California, 1995.
[8] D. F. Gaitan *et al.*, Phys. Rev. E **54**, 525 (1996).
[9] C. C. Wu and P. H. Roberts, Phys. Rev. Lett. **70**, 3424 (1993).
[10] C. C. Wu and P. H. Roberts, Proc. R. Soc. London, Ser. A **445**, 323 (1994).
[11] H. P. Greenspan and A. Nadim, Phys. Fluids A **5**, 1065 (1993).
[12] L. A. Crum, J. Acoust. Soc. Am. **95**, 559 (1994).
[13] W. C. Moss, D. B. Clarke, J. W. White, and D. A. Young, Phys. Fluids **6**, 2979 (1994).
[14] L. Kondić, J. I. Gersten, and C. Yuan, Phys. Rev. E **52**, 4976 (1995).
[15] L. Kondić, Ph.D. thesis, The City University of New York, 1995.
[16] J. Glanz, Science **274**, 719 (1996).
[17] B. P. Barber, R. A. Hiller, R. Löfstedt, S. J. Putterman, and K. Weninger, Phys. Rep. **281**, 65 (1997).
[18] J. N. Kordomenos, M. Bernard, and B. Denardo, J. Acoust. Soc. Am. **100**, 2717 (1996).
[19] K. Weninger, S. J. Putterman, and B. P. Barber, Phys. Rev. E **54**, R2205 (1996).
[20] V. Q. Vuong and A. J. Szeri, Phys. Fluids **8**, 2354 (1996).
[21] H. Kwak and H. Yang, J. Phys. Soc. Jpn. **64**, 1980 (1995).
[22] H. Kwak and J. H. Na, Phys. Rev. Lett. **77**, 4454 (1996).
[23] K. Yasui, J. Acoust. Soc. Am. **98**, 2772 (1995).
[24] K. Yasui, J. Phys. Soc. Jpn. **65**, 2830 (1996).
[25] K. Yasui, Ph.D. thesis, Waseda University, 1996.
[26] K. Yasui, J. Phys. Soc. Jpn. **66**, 2911 (1997).
[27] D. Lohse, M. P. Brenner, T. F. Dupont, S. Hilgenfeldt, and B. Johnston, Phys. Rev. Lett. **78**, 1359 (1997).
[28] B. P. Barber, K. Weninger, R. Löfstedt, and S. J. Putterman, Phys. Rev. Lett. **74**, 5276 (1995).
[29] R. Hiller, K. Weninger, S. J. Putterman, and B. P. Barber, Science **266**, 248 (1994).

[30] R. G. Holt and D. F. Gaitan, Phys. Rev. Lett. **77**, 3791 (1996).
[31] A. Eller and H. G. Flynn, J. Acoust. Soc. Am. **37**, 493 (1965).
[32] T. G. Leighton, *The Acoustic Bubble* (Academic, London, 1994).
[33] F. R. Young, J. Acoust. Soc. Am. **60**, 100 (1976).
[34] P. W. Atkins, *Physical Chemistry*, 2nd ed. (Oxford University, New York, 1982).
[35] M. N. Kogan, *Rarefied Gas Dynamics* (Plenum, New York, 1969), p. 385.
[36] V. Kamath, A. Prosperetti, and F. N. Egolfopoulos, J. Acoust. Soc. Am. **94**, 248 (1993).
[37] G. A. Cook, *Argon, Helium and the Rare Gases* (Interscience, New York, 1961), Vol. 1.
[38] R. W. Schrage, *A Theoretical Study of Interphase Mass Transfer* (Columbia University Press, New York, 1953).
[39] S. Fujikawa and T. Akamatsu, J. Fluid Mech. **97**, 481 (1980).
[40] M. Matsumoto (private communication).
[41] J. O. Hirschfelder, C. F. Curtiss, and R. B. Bird, *Molecular Theory of Gases and Liquids* (Wiley, New York, 1954).
[42] Y. S. Touloukian and T. Makita, *Specific Heat* (IFI/Plenum, New York, 1970).
[43] B. P. Barber and S. J. Putterman, Phys. Rev. Lett. **69**, 3839 (1992).
[44] D. L. Baulch *et al.*, *Evaluated Kinetic Data for High Temperature Reactions* (Butterworths, London, 1972), Vol. 1; *Evaluated Kinetic Data for High Temperature Reactions* (Butterworths, London, 1973), Vol. 2; *Evaluated Kinetic Data for High Temperature Reactions* (Butterworths, London, 1976), Vol. 3.
[45] K. R. Weninger, B. P. Barber, and S. J. Putterman, Phys. Rev. Lett. **78**, 1799 (1997).
[46] M. R. Spiegel, *Theory and Problems of Calculus of Finite Differences and Difference Equations* (McGraw-Hill, New York, 1971).